Atmospheric and Oceanic Science Letters 14 (2021) 100025

Contents lists available at ScienceDirect

Atmospheric and Oceanic Science Letters

journal homepage:
http://www.keaipublishing.com/en/journals/atmospheric-and-oceanic-science-letters/

A high-top version of IAP-AGCM: Preliminary assessment and sensitivity IAP-AGCM
中高层大气环流模式的初步评估与敏感性分析

Zhaoyang Chai [a,b], Minghua Zhang [c,*], Qingcun Zeng [a,b], He Zhang [a,b], Jiangbo Jin [a,b], Jinbo Xie [d], Ting You [b,e]

[a] International Center for Climate and Environment Sciences, Institute of Atmospheric Physics, Chinese Academy of Sciences, Beijing, China
[b] College of Earth and Planetary Science, University of Chinese Academy of Sciences, Beijing, China
[c] School of Marine and Atmospheric Sciences, State University of New York at Stony Brook, NY, USA
[d] State Key Laboratory of Numerical Modeling for Atmospheric Sciences and Geophysical Fluid Dynamics, Institute of Atmospheric Physics, Chinese Academy of Sciences, Beijing, China
[e] Center for Monsoon System Research, Institute of Atmospheric Physics, Chinese Academy of Sciences, Beijing, China

ARTICLE INFO

Key words:
IAP-AGCM
Middle atmosphere
Stratosphere
Radiative heating
Transient heat flux
关键词:
IAP-AGCM
中层大气
平流层
辐射加热
瞬变涡动热通量

ABSTRACT

Extending the atmospheric model top to high altitude is important for simulation of upper atmospheric phenomena, such as the stratospheric quasi-biennial oscillation. The high-top version of the Institute of Atmospheric Physics Atmospheric General Circulation Model with 91 vertical layers (IAP-AGCML91) extends to the mesopause at about 0.01 hPa (~80 km). The high-top model with a fully resolved stratosphere is found to simulate a warmer stratosphere than the low-top version, except near the South Pole, thus reducing its overall cold bias in the stratosphere, and significantly in the upper stratosphere. This sensitivity is shown to be consistent with two separate mechanisms: larger shortwave heating and larger poleward stratospheric meridional eddy heat flux in the high-top model than in the low-top model. Results indicate a significant influence of vertical resolution and model top on climate simulations in IAP-AGCM.

摘要

提高大气环流模式的模式顶层高度对中高层大气 (如平流层准两年振荡) 的准确模拟至关重要. 本研究将IAP大气环流模型 (IAP-AGCM) 延伸至中层大气顶 (~0.01 hPa, ~80 km) 并提高垂直方向分辨率 (91层) , 发展了一个中高层大气环流模型 (IAP-AGCML91) . 结果表明, 与低层模式相比, 该中高层大气模式在整体上显著减小了平流层尤其是上平流层的冷偏差.研究发现这种改善与两种机制有关:与低层模式相比, 高层模式模拟的短波加热更大, 极区平流层附近的经向涡动热通量更大.上述结果表明, 垂直分辨率和模式顶层高度对IAP-AGCML91的气候模拟有重要影响.

1. Introduction

Stratosphere-resolved models help to improve the simulation of stratospheric climatology (Pawson et al., 2000; Cordero and Forster, 2006). Many studies have shown that both internal stratospheric climate variability and external stratospheric climate forcing play an important role in driving tropospheric climate (Gerber et al., 2012), which has become another motivation to increase the stratospheric representation in climate models. Besides, changes in the stratospheric climate also have a significant effect on the pattern and magnitude of regional tropospheric climate (Sigmond and Scinocca, 2010; Scaife et al., 2012; Karpechko and Manzini, 2012). Therefore, it is necessary to realistically resolve the stratospheric processes in climate models to improve the simulation of basic states and variabilities in the stratosphere.

In the Coupled Model Intercomparison Projects (CMIPs), from phase 3 (CMIP3) to five (CMIP5) and six (CMIP6), which is in progress, it is a major trend to increase the number of vertical levels and the model top altitude in the atmospheric component of coupled climate models to represent a more realistic stratosphere in general circulation models. For example, only 5 of the 23 CMIP3 models had model tops above 1 hPa (Cordero and Forster, 2006), but this ratio increased to 15 of 45 models in CMIP5. Besides, more than half (~75 entries) of the 128 entries participating in CMIP6 have model tops above 1 hPa up to now (https://wcrp-cmip.github.io/CMIP6_CVs/docs/CMIP6_source_id.html). A model top above 1 hPa with a relatively high vertical resolution can better repre-

* Corresponding author.
E-mail address: minghua.zhang@stonybrook.edu (M. Zhang).

https://doi.org/10.1016/j.aosl.2020.100025
Available online 26 December 2020

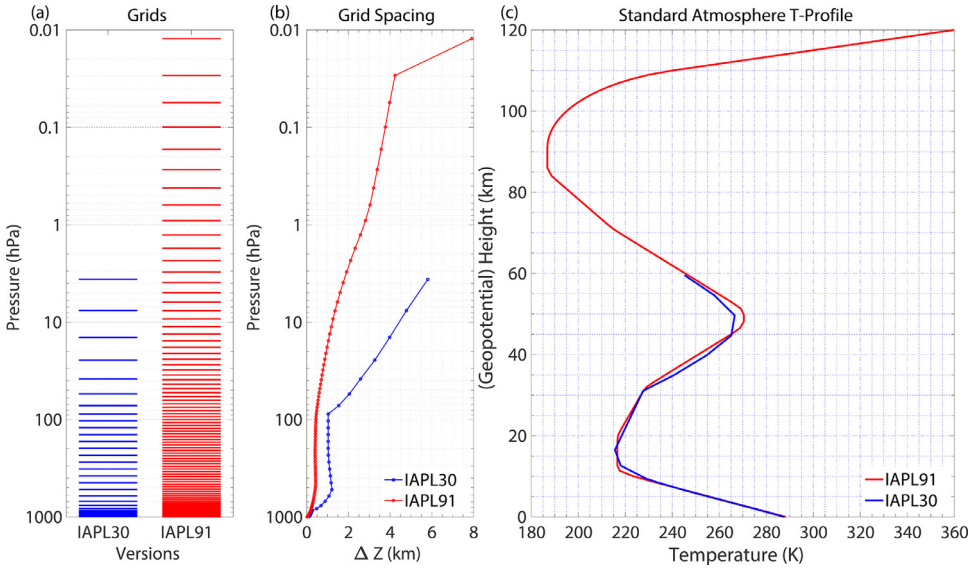

Fig. 1. (a) Hybrid vertical coordinate and (b) vertical grid spacing used in different versions of IAP-AGCM simulations: IAPL30 (blue line), and IAPL91 (red line). (c) Vertical temperature (units: K) profile of standard atmosphere employed in the old default version of IAPL30 (blue line) and in the newly designed version of IAPL91 (red line). The *y*-coordinate is geopotential height below 84.852 km and geometric height above 86 km, noting that 84.852 geopotential km equals 86 geometric km. This profile takes U.S. Standard Atmosphere 1976 as a reference, with some smoothing modifications.

sent the stratospheric variability and yield a more realistic stratosphere–troposphere interaction, such as the long-lasting tropospheric impacts of the Northern Annular Mode (Charlton-Perez et al., 2013).

However, there was no high-top model above 1 hPa from China before CMIP5, and in the recent registered entries of CMIP6, only BCC-CSM2-HR (Beijing Climate Center, Climate System Model, High Resolution) has a model top of 0.1 hPa with 56 vertical levels (Xin et al., 2019), lacking the representation of interaction between the upper and lower middle atmosphere. Besides, in the Institute of Atmospheric Physics Atmospheric General Circulation Model (IAP-AGCM), the previous version of the atmospheric component (IAP-AGCM 4.1) of the Chinese Academy of Sciences Earth System Model (CAS-ESM) was not able to fully represent the stratospheric processes owing to its low model top of 2.26 hPa (~40 km). Furthermore, models with a model top below the stratopause and with a low vertical resolution fail to properly simulate episodic stratospheric variability such as the quasi-biennial oscillation (Richter et al., 2014), indicating the need to increase the model top and vertical resolution to fully resolve the stratosphere in IAP-AGCM.

Therefore, we developed a high-top version of IAP-AGCM with 91 vertical layers (IAP-AGCML91) based on IAP-AGCM 4.1, which includes a new stratification profile of standard atmosphere. The model extends upward to about 0.01 hPa (~80 km) with a finer vertical resolution. In this paper, we focus on a preliminary assessment of the performance of the newly designed IAP-AGCML91.

The paper is organized as follows. The models and experimental design are briefly described in Section 2. The results from simulations and analyses are presented in Section 3. Finally, a summary and discussion of the key findings is provided in section 4.

2. Model description and experiments

2.1. Model description

The development of IAP-AGCM has evolved through a series of versions, including a 2-level model (Zeng et al., 1989); 9-level model (Zhang, 1990; Bi, 1993; Liang, 1996); 26-level model (Zhang et al., 2009; Zhang, 2009), which is IAP-AGCM 4.0; and the latest 35-level model, IAP-AGCM 5.0 (Zhang et al., 2020). The present study used IAP-AGCM 4.1, the complete details of which are described in Zhang (2009), Sun et al., (2012), and Zhang et al., (2013). IAP-AGCM 4.1 uses the full physical package from CAM5 with only minor adjustments to certain parameters. Additionally, the parameterization of gravity waves only specifies the orographic source, following McFarlane (1987).

IAP-AGCM 4.1 uses a horizontal resolution of about 1.4° latitude by 1.4° longitude and 30 vertical layers (IAPL30 hereafter) with the model top at ~ 2.26 hPa, based on which, a high-top version of IAP-AGCM was developed with 91 vertical layers (IAPL91 hereafter) reaching to the mesopause at 0.01 hPa (~80 km). Hybrid vertical coordinates of the two versions are shown in Fig. 1(a). IAPL91 has a relatively high vertical resolution with vertical spacings of less than 400 m below 500 hPa, ~400 m between 500 and 100 hPa, and increasing from ~400 to ~8000 m above 100 hPa (Fig. 1(b)). The model is expected to better resolve atmospheric waves, which play an important role in the variabilities of the stratosphere and mesosphere via wave–mean-flow interactions. We incorporated a new temperature profile for standard stratification deduction extending upward to ~120 km, making up for the deficiency above 60 km in the default version of IAP-AGCM (Fig. 1(c)). This new profile takes US Standard Atmosphere 1976 as a reference, with some smoothing modifications using the cubic B-spline method and the cubic Akima-spline method.

Table 1 Summary of experiments and simulations.

Experiment	Model levels	Model top (hPa)	Run type	Period
L30AD	30	2.26	ADIAB	365 days
L91AD	91	0.01	ADIAB	365 days
L30	30	2.26	AMIP	1979–2005
L91	91	0.01	AMIP	1979–2005
L30ID	30	2.26	IDEAL	0001–0010
L91ID	91	0.01	IDEAL	0001–0010

2.2. Experiment and simulation

The experiments examined in this paper are briefly outlined in Table 1. In order to verify the new dynamical core with the new profile, Rossby–Haurwitz (RH) waves with wavenumber 4 (Zhang, 1990, 2009; Giraldo and Rosmond, 2004) were used to initialize models, integrating for 365 days in both IAPL30 and IAPL91, referred to as L30AD and

L91AD, respectively, which are generally employed to test the stability of a dynamical core. The AMIP (Atmospheric Model Intercomparison Project) simulations of IAPL30 and IAPL91 with the new profile are referred to as L30 and L91, carried out from 1979 to 2005 with prescribed observed global Hadley Centre Sea Surface Temperature and Sea Ice (Taylor, Stouffer, and Meehl, 2009). Also, the Held–Suarez (HS) method (Held and Suarez, 1994; Zhang, Zhang, and Zeng, 2013) was used in both IAPL30 and IAPL91, referred to as L30ID and L91ID, respectively, which is generally employed to test model performance without moist physics but with only idealized physical forcing including Newtonian relaxation of temperature and surface Rayleigh damping of wind. All analyses are based on the monthly mean and daily mean output by models and the monthly means of daily means data from the ERA-Interim dataset (ERAI).

3. Results

3.1. RH tests for the dynamical core with the new profile

To test the dynamical framework of IAP-AGCM with the new profile, we used baroclinic RH waves with zonal wavenumber 4 to initialize the 30-layer and 91-layer versions and integrated for 365 days, respectively. Fig. 2 shows the evolution of the RH wave via its horizontal distribution of the initial, 60th day, 80th day, and 365th day zonal wind at 500 hPa. The initial wave patterns for L30AD and L91AD are the same, with maximum zonal wind of ~15.9 m s^{-1}. The wave patterns for both simulations are kept well to the 60th day, are slightly deformed on the 80th day due to the damping effect of numerical schemes (Zhang, 2009), and are almost damped on the 365th day with a relatively homogeneous distribution over latitudes. These results are consistent with the default 30-layer version (Zhang, 2009), validating the dynamical core with the new profile in both the 30-layer and 91-layer models.

3.2. Sensitivity of simulated temperature in the two model versions

3.2.1. Temperature difference between low-top and high-top versions

Fig. 3(a–c) shows latitude–pressure cross sections of temperature from ERAI, L30, and L91, respectively, along with their differences shown in Fig. 3(d–f). The model results are from AMIP simulations from 1979 to 2005. Dotted shading indicates differences judged statistically significant at the 0.05 level for a Student's *t*-test based on 324 monthly means. The overall temperature structures are captured by both L30 (Fig. 3(b)) and L91 (Fig. 3(c)), with a cold (~190 K) tropical tropopause. However, L91 reproduces the warm peak at the stratopause near ~1 hPa, which is not presented in L30. Furthermore, L91 simulates a warmer stratosphere than L30, except near the South Pole, thus reducing its overall cold bias in the stratosphere (Fig. 3(d)). This reduction in cold bias is statistically significant in the upper stratosphere (1–10 hPa) but not as significant in the lower stratosphere (10–100 hPa). The cold bias in the northern polar stratosphere from L30 is reduced to some extent in L91, while the cold bias in the southern polar stratosphere from L30 is enlarged by ~2–4 K poleward of 60°S in L91 (Fig. 3(d)). Actually, this cold bias is more evident in winter of the Southern Hemisphere (SH) (Figs. S1 and S2). Besides, L91 simulates a colder troposphere than L30, enlarging its cold bias by up to 2 K (Fig. 3(d)). We have found that the temperature difference in the stratosphere between the two versions is consistent with two separate mechanisms: shortwave radiative heating and convergence of eddy heat transport, which are respectively described in following sections.

3.2.2. Stratospheric heating by solar radiation

Fig. 4(a–c) shows latitude–pressure cross sections of the shortwave radiative heating rate from L30, L91, and their difference (L91 minus L30). L91 simulates an overall larger solar heating rate in the upper stratosphere above 20 hPa than L30, with a peak at the tropical stratopause near ~1 hPa, which is not presented in L30. This larger heating rate may play an important role in directly heating the stratosphere, especially at low and middle latitudes with large magnitude, which leads to a higher temperature in this region. The solar radiative heating rate in most of the atmosphere below 20 hPa simulated by L91 is a little smaller than that from L30, which may explain the colder troposphere in L91.

In the stratosphere, the shortwave heating is mainly due to the absorption of ozone. The vertical distributions of ozone interpolated by L30 (top level of ~3.64 hPa) and L91 (top level of ~0.01 hPa) from the prescribed ozone profile are almost the same below its top level of ~3.54 hPa (Fig. S8(a)). However, L91 interpolates a much smaller ozone concentration at the top level than L30 due to its higher model top, i.e., ~0 ppmv at ~0.01 hPa in L91 versus ~8 ppmv at ~3.64 hPa in L30 (Fig. S8(a)). Furthermore, in the radiative calculation, there is another layer between TOM (top of model) and TOA (top of atmosphere), where the atmospheric properties are specified as those in the top layer of the model, including the concentration of absorbing constituents. This cruder approximation leads to a smaller ozone concentration in this added layer in L91 (~0 ppmv) than that in L30 (~8 ppmv). Thus, the ozone concentration for L91 decreases from ~8 to ~0 ppmv with the height increasing from 3.54 hPa to TOA, while the ozone concentration for L30 maintains a constant of ~8 ppmv (Figure S8a). This indicates less radiative absorption above 3.54 hPa, allowing more solar heat energy into the atmosphere below 3.54 hPa in L91 (Fig. S8(b)). Less solar energy is absorbed above 3.54 hPa, but more energy is absorbed below 3.54 hPa, resulting in the larger solar heating in the stratosphere in L91. The difference in the solar heating between the two models indicates that substantial improvements are needed in the low-top model near the model top.

3.2.3. Polar stratospheric heating by transient eddies

Heat transport by eddies is an important mechanism to maintain the energy balance indicated between low latitudes and high latitudes, which is shown in Fig. 4(d–f). The heat flux by transient eddies is calculated as (Zhang et al., 2013)

$$\overline{v'T'} = \overline{vT} - \overline{v}\,\overline{T},$$

where v is meridional velocity and T is temperature, the overbar denotes the monthly mean, and the prime denotes the deviation from the mean. L30 (Fig. 4(d)) and L91 (Fig. 4(e)) both capture the two peaks of poleward heat fluxes in the lower and upper troposphere at middle latitudes. Besides, one more peak exists in the stratosphere at about 10 hPa near 60°S/N in L30, which shifts upward higher near the stratopause in L91 due to its higher model top. The stronger peak near the stratopause in L91 transports more heat energy from low latitudes to high latitudes and the convergence warms the polar upper stratosphere (Fig. 4(f)), for the heat transport is equivalent to an integrated heating rate from the poles. This mechanism is effective in the Northern Hemisphere (NH) but not as effective in the SH where the polar stratosphere gets apparently colder in L91 (Fig. 3(d)), which may be associated with the position of the maximum heat flux. There is an obvious asymmetry for the stratospheric distribution of heat flux between the hemispheres both in L91 (Fig. 4(e)) and in L30 (Fig. 4(d)), and the peak stratospheric heat flux is much closer to the pole in the NH than in the SH. For the regions poleward of 70°S, the integrated heating rate due to the convergence of heat flux for SH is

$$\frac{\partial}{\partial t}\int_{90°\mathrm{S}}^{70°\mathrm{S}} \bar{T}\,\mathrm{d}y = \left(\overline{v'T'}\right)_{90°\mathrm{S}} - \left(\overline{v'T'}\right)_{70°\mathrm{S}} = \left|\overline{v'T'}\right|_{70°\mathrm{S}},$$

for $(\overline{v'T'})_{90°\mathrm{S}}$ is close to zero. The peak of $\overline{v'T'}$ in the stratosphere locates at ~55°S in the SH versus ~65°N in the NH (Fig. 4e(d, e)). If the peak of $\overline{v'T'}$ in the SH shifts poleward from ~55°S to ~65°S, $|\overline{v'T'}|_{70°\mathrm{S}}$ will become larger and then the heating rate $\frac{\partial}{\partial t}\int_{90°\mathrm{S}}^{70°\mathrm{S}} \bar{T}\,\mathrm{d}y$ will be larger.

As a result, the cold bias in the northern polar stratosphere from L30 is reduced in L91, possibly due to the larger convergence of heat transport, while it seems ineffective in the SH. We do not have a clear

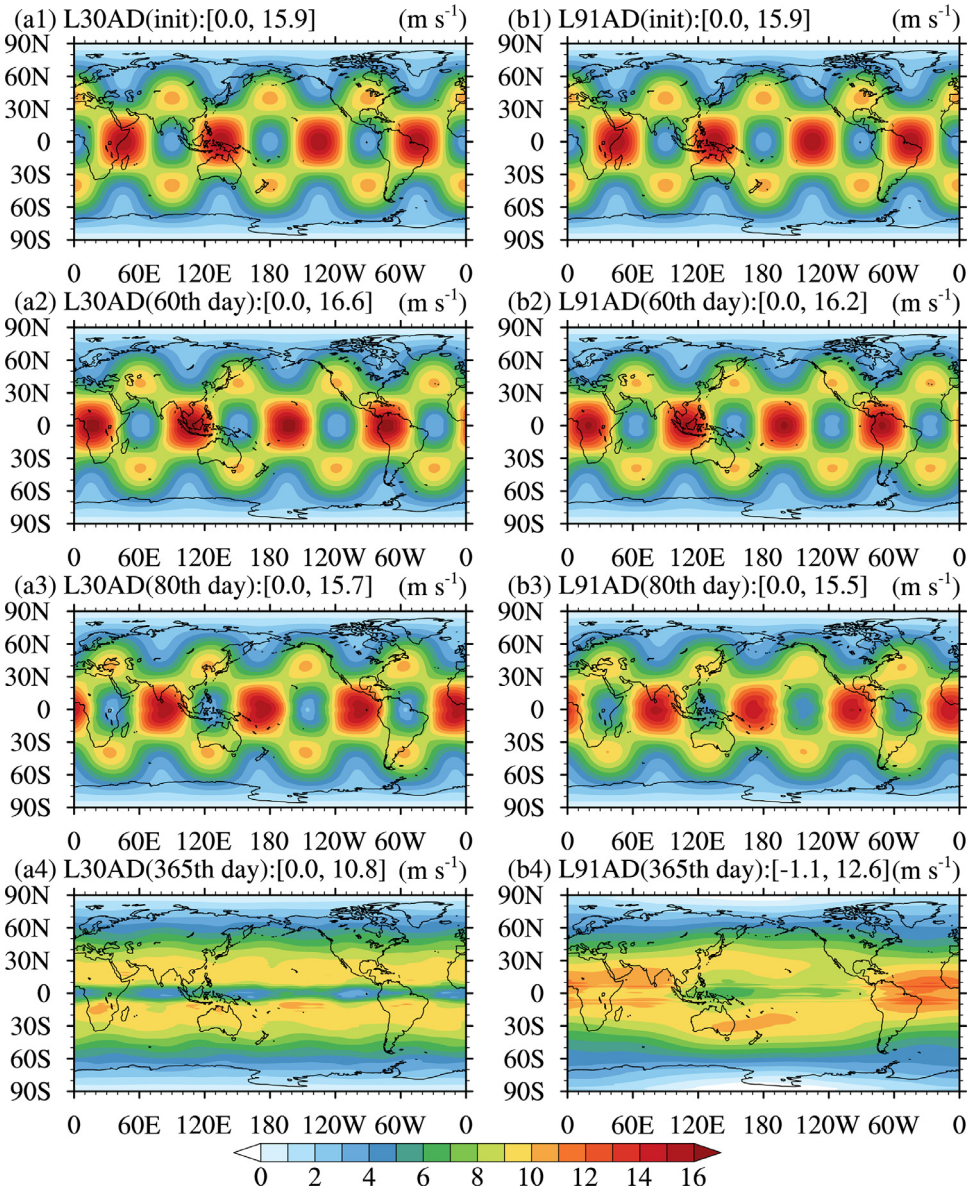

Fig. 2. Longitude–latitude cross sections of daily mean zonal wind (color shading; units: m s^{-1}) at 500 hPa simulated by L30AD (left) and L91AD (right), showing the evolution of the RH wave with wavenumber 4 via its horizontal distributions of the (a1, b1) initial day, (a2, b2) 60th day, (a3, b3) 80th day, and (a4, b4) 365th day for L30AD and L91AD, respectively. Contour intervals are 1 m s^{-1}. Maximum and minimum values (rounded) of zonal wind are given in the square brackets on the top side of each plot.

explanation as to why the cold bias in the southern polar stratosphere is larger in the L91 model even though the convergence of heat transport is larger and solar heating is also larger.

The cause of the stronger eddy activities in the high-top model in the stratosphere is likely due to the specification of the horizontal diffusion used in the dynamical core. In IAP AGCM4, the horizontal diffusion is a linear ∇^2 form with coefficient 2.5×10^5 m^2 s^{-1} in the top three layers of the model and a linear ∇^4 form with coefficient 1.0×10^{15} m^4 s^{-1} elsewhere. For waves larger than 1000 km, the damping in the low-top model is orders of magnitude larger near the model top than that in the high-top model at the same pressure level. Therefore, the wave activities in the stratosphere are weaker in the high-top model.

3.2.4. Transient eddy heat flux simulated with idealized physics

To confirm the difference in heat transport of the full model between the two versions, we next examine the impact of the dynamical core with idealized physics by using HS experiments (L30ID and L91ID), which were integrated for 10 years with the last 9 years used. The so-called idealized physics simulation denotes no moist processes, no topography, no land–sea contrast, and no seasonal or diurnal cycle.

In Fig. 5(a, b), the major features of the real atmospheric temperature are reproduced, similar to the climate simulations shown in Fig. 3(b, c). However, L91ID simulates a colder stratosphere in the tropics and a warmer stratosphere at high latitudes than L30ID ((Fig. 5(c))), which may be directly linked with the stronger heat transport by eddies in the upper stratosphere at high latitudes in L91ID (Fig. 5(f)). The stronger heat flux in the high-top version is consistent with the result of the climate simulation shown in Fig. 4(f). The difference in the heat transport between the two versions is likely related to less numerical damping near the stratopause in the high-top model. Both the simulations of the heat flux without moist physics present a very good symmetry between the two hemispheres (Fig. 5(d, e)), which differs from the results with full physics shown in Fig. 4(d, e), indicating the effects of moist physics. With idealized physics, the stratospheric peaks in both hemi-

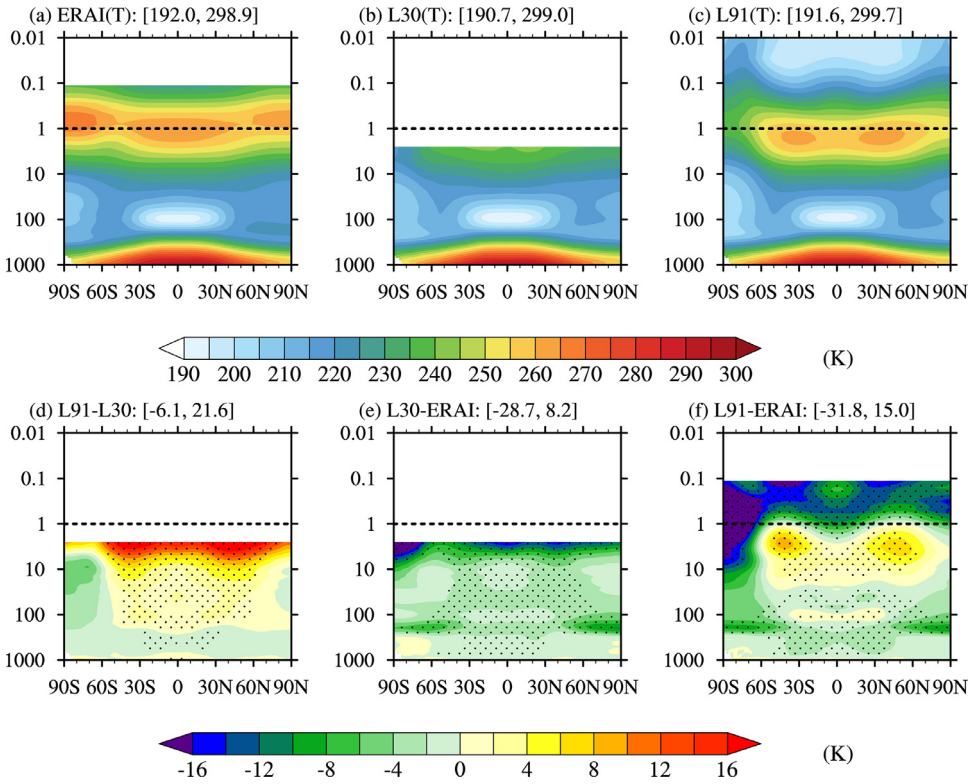

Fig. 3. Latitude–pressure (units: hPa) cross sections of zonally averaged 27-yr (1979–2005; AMIP) annual mean temperature (color shading; units of K) from (a) ERAI, (b) L30 and (c) L91, and the biases of (e) L30 and (f) L91 in contrast to ERAI, and (d) the difference between the two simulations (L91 minus L30). Contour intervals are 5 K in (a–c) and 2 K in (d–f). Dotted shading indicates statistically significant areas at the 0.05 level according to the Student's *t*-test based on 324 monthly means. Maximum and minimum values (rounded) are given in the square brackets on the top side of each plot.

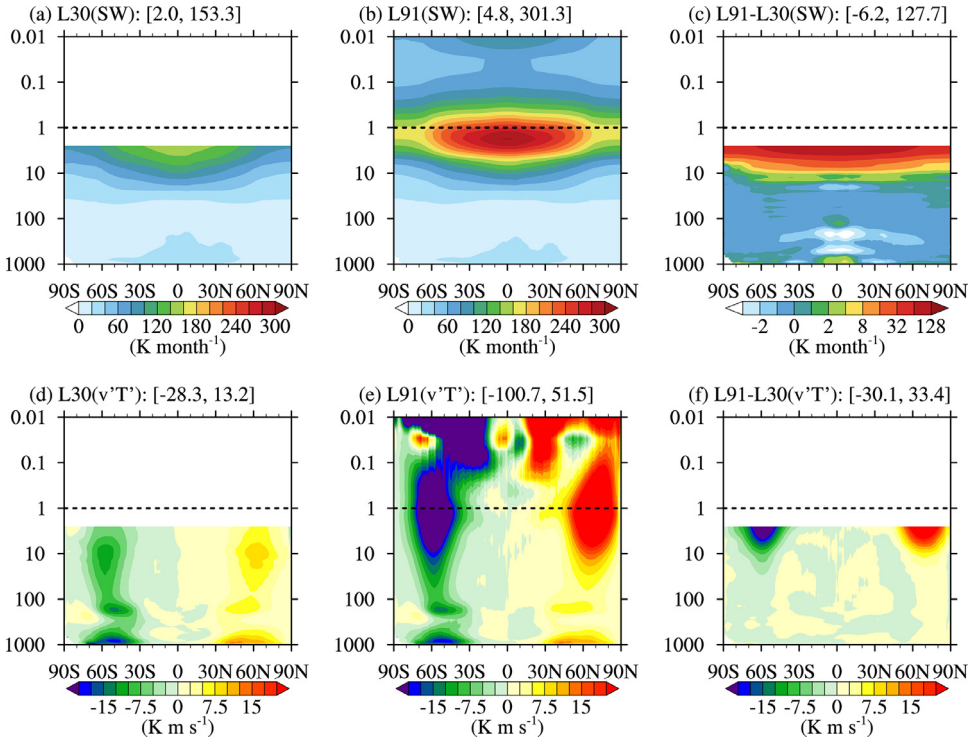

Fig. 4. Latitude–pressure (units: hPa) cross sections of zonally averaged 27-yr (1979–2005; AMIP) annual mean solar heating rate (color shading; units: K/month) from (a) L30 and (b) L91, and (c) their difference (L91 minus L30); and the corresponding transient eddy heat flux (color shading; units: K m s^{-1}) from (d) L30 and (e) L91, and (f) their difference (L91 minus L30). Contour intervals are 20 K/month in (a, b) and 2.5 K m s^{-1} in (d–f). Contours are (−4, −2, −1, 0, 1, 2, 4, 8, 16, 32, 64, 128) K/month in (c). Maximum and minimum values (rounded) are given in the square brackets on the top side of each plot.

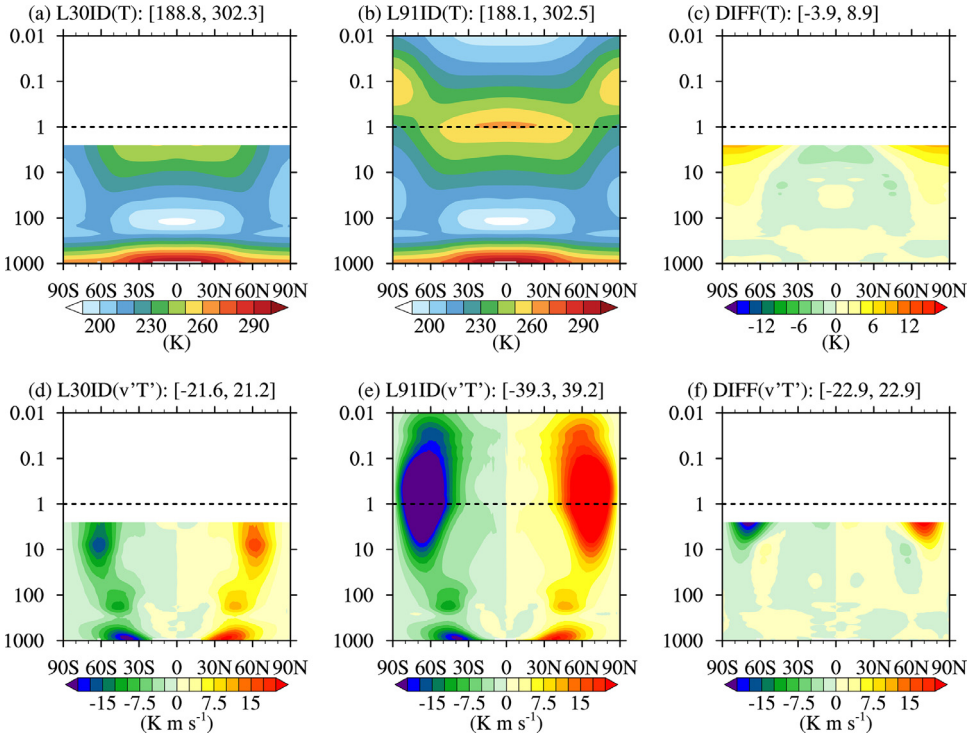

Fig. 5. Latitude–pressure (units: hPa) cross sections of zonally averaged 9-yr (0002–0010; IDEAL) annual mean temperature (color shading; units: K) from (a) L30ID, (b) L91ID, and (c) their difference (L91ID minus L30ID); and the corresponding transient eddy heat flux (color shading; units: K m s^{-1}) from (d) L30ID, (e) L91ID, and (f) their difference (L91ID minus L30ID). Contour intervals are 10 K in (a, b), 2 K in (c), and 2.5 K m s^{-1} in (d–f). Maximum and minimum values (rounded) are given in the square brackets on the top-left side of each plot.

spheres are quite close to the poles and the convergence contributes to increasing the temperature in the polar stratosphere (Fig. 5(d, e)), while in the full model the peak in the SH is far from the South Pole, leading to a colder southern polar stratosphere. The asymmetry shown in Fig. 4(d, e) indicates different responses of transient eddies to the moist physics between the two hemispheres, which needs to be further investigated.

4. Summary and discussion

We developed a high-top version of IAP-AGCM based on IAP-AGCM 4.1, with the model top reaching the mesopause at 0.01 hPa (~80 km) to include the middle atmosphere. It has 91 vertical levels, including a newly designed stratification profile of standard atmosphere. We validated the dynamical core with the new profile via RH tests using both 30-layer and 91-layer versions. The high-top model with a fully resolved stratosphere simulates a warmer stratosphere than the low-top version, except near the South Pole, thus reducing its overall cold bias in the stratosphere, and significantly in the upper stratosphere. This sensitivity is consistent with two separate mechanisms: larger shortwave heating and larger convergence of stratospheric meridional eddy heat flux in the high-top version than those in the low-top version.

The difference in the solar heating between the two models in the upper stratosphere may be linked with the cruder approximation of radiative calculation in the low-top model in the stratosphere near the model top. The larger poleward stratospheric meridional eddy heat flux in the high-top version transmits more heat from the tropics to high latitudes, the convergence of which reduces the cold bias in the northern polar stratosphere. However, this mechanism seems not as effective in SH partly because the peak of heat flux is not as close to the pole as in the NH. We do not have a clear explanation for the larger cold bias in the southern polar stratosphere in the high-top model even though both the convergence of eddy transport of heat and solar heating are larger. Besides, the stronger heat flux in high-top version is likely associated with less damping due to horizontal diffusion near the stratopause in the high-top model. These results indicate a significant influence of vertical resolution and model top on both the dynamical core and physical processes, which may be a source of uncertainty in climate simulations in IAP-AGCM.

In future work, we will further assess the sensitivities of temperature to the vertical resolution and model top. The impacts of vertical resolution and model top will be separated to obtain clearer explanations for the larger cold bias in the southern polar stratosphere in the high-top model. Additionally, the zonal wind (Figs, S3–S7) simulated by the high-top model needs to be further investigated to make a more complete assessment of the model.

Funding

This research was supported by the National Natural Science Foundation of China [grant number 41991282], the National Major Research High Performance Computing Program of China [grant number 2016YFB0200800], the National Natural Science Foundation of China [grant numbers 41630530 and 41706036], and the National Key Scientific and Technological Infrastructure project "Earth System Science Numerical Simulator Facility" (EarthLab).

Acknowledgments

We gratefully acknowledge Dongling ZHANG for assistance with computing resources to facilitate the development of IAP-AGCM.

Supplementary materials

Supplementary material associated with this article can be found, in the online version, at doi:10.1016/j.aosl.2020.100025.

References

Bi, X.Q., 1993. An improved nine-level atmospheric general circulation model and its application to climate simulation. Institute of Atmospheric Physics, Chinese Academy of Sciences.

Charlton-Perez, A.J., Baldwin, M.P., Birner, T., Black, R.X., Butler, A.H., Calvo, N., Davis, N.V., et al., 2013. On the lack of stratospheric dynamical variability in low-top versions of the CMIP5 models. J. Geophys. Res. 118 (6), 2494–2505. doi:10.1002/jgrd.50125.

Cordero, E.C., Forster, P.M.D., 2006. Stratospheric variability and trends in models used for the IPCC AR4. Atmos. Chem. Phys. 6, 5369–5380. doi:10.5194/acp-6-5369-2006.

Gerber, E.P., Butler, A., Calvo, N., Charlton-Perez, A., Giorgetta, M., Manzini, E., Perlwitz, J., et al., 2012. Assessing and understanding the impact of stratospheric dynamics and variability on the earth system. Bull. Am. Meteorol. Soc. 93 (6), 845–859. doi:10.1175/BAMS-D-11-00145.1.

Giraldo, F.X., Rosmond, T.E., 2004. A scalable spectral element Eulerian atmospheric model (SEE-AM) for NWP: dynamical core tests. Monthly Weather Rev. 132 (1), 133–153. doi:10.1175/1520-0493(2004)132<0133:ASSEEA>2.0.CO;2.

Held, I.M., Suarez, M.J., 1994. A proposal for the intercomparison of the dynamical cores of atmospheric general circulation models. Bull. Am. Meteorol. Soc. 75 (10), 1825–1830. doi:10.1175/1520-0477(1994)075<1825:APFTIO>2.0.CO;2.

Karpechko, A.Y., Manzini, E., 2012. Stratospheric influence on tropospheric climate change in the Northern Hemisphere. J. Geophys. Res. 117, D05133. doi:10.1029/2011JD017036.

Liang, X.Z., 1996. Description of a nine-level grid point atmospheric general circulation model. Adv. Atmos. Sci. 13 (3), 269–298 doi:CNKI:SUN:DQJZ.0.1996-03-000.

McFarlane, N.A., 1987. The effect of orographically excited gravity wave drag on the general circulation of the lower stratosphere and troposphere. J. Atmos. Sci. 44 (14), 1775–1800. doi:10.1175/1520-0469(1987)044<1775:TEOOEG>2.0.CO;2.

Pawson, S., Kodera, K., Hamilton, K., Shepherd, T.G., Beagley, S.R., Boville, B.A., Langematz, U., et al., 2000. The GCM-Reality Intercomparison Project for SPARC (GRIPS): Scientific issues and initial results. Bull. Am. Meteorol. Soc. 81 (4), 781–796. doi:10.1175/1520-0477(2000)081<0781:TGIPFS>2.3.CO;2.

Richter, J.H., Solomon, A., Bacmeister, J.T., 2014. On the simulation of the quasi-biennial oscillation in the Community Atmosphere Model, version 5. J. Geophys. Res. 119 (6), 3045–3062. doi:10.1002/2013JD021122.

Scaife, A.A., Spangehl, T., Fereday, D.R., Cubasch, U., Langematz, U., Akiyoshi, H., Gettelman, A., et al., 2012. Climate change projections and stratosphere-troposphere interaction. Clim. Dyn. 38 (9-10), 2089–2097. doi:10.1007/s00382-011-1080-7.

Sigmond, M., Scinocca, J.F., 2010. The influence of the basic state on the Northern Hemisphere circulation response to climate change. J. Clim. 23 (6), 1434–1446. doi:10.1175/2009JCLI3167.1.

Sun, H.C., Zhou, G.Q., Zeng, Q.C., 2012. Assessments of the climate system model (CAS-ESM-C) using IAP AGCM4 as its atmospheric component. [In Chinese.]. Chin. J. Atmo. Sci. 36 (2), 215–233. doi:10.3878/j.issn.1006-9895.2011.11062.

Taylor, K.E., Stouffer, R.J., Meehl, G.A., 2009. An overview of CMIP5 and the experiment design. Bull. Am. Meteorol. Soc. 93 (4), 485–498. doi:10.1175/BAMS-D-11-00094.1.

Xin, X.G., Wu, T.W., Zhang, J., Zhang, F., Li, W.P., Zhang, Y.W., Lu, Y.X., et al., 2019. Introduction of BCC models and its participation in CMIP6. [In Chinese.]. Clim. Change Res. 15 (5), 533–539. doi:10.12006/j.issn.1673-1719.2019.039.

Zeng, Q. C., X. H. Zhang, X. Z. Liang, C. G. Yuan, and S. F. Chen. 1989. "Documentation of IAP two-level atmospheric general circulation model." DOE/ER/60314-H1, TR044, 383pp.

Zhang, H., Lin, Z.H., Zeng, Q.C., 2009. The computational scheme and the test for dynamical framework of IAP AGCM-4. [In Chinese.]. Chin. J. Atmos. Sci. 33 (6), 1267–1285. doi:10.3878/j.issn.1006-9895.2009.06.13.

Zhang, H., Zhang, M., Jin. K. Fei, J., Ji, D., Wu, C., Zhu, J., et al., 2020. CAS-ESM 2: Description and climate simulation performance of the Chinese academy of sciences (CAS) earth system model (ESM) version 2.. J. Adv. Modeling Earth Syst. doi:10.1029/2020MS002210.

Zhang, H., 2009. Development of IAP atmospheric general circulation model version 4.0 and its climate simulations. Institute of Atmospheric Physics, Chinese Academy of Sciences.

Zhang, H., Zhang, M.H., Zeng, Q.C., 2013. Sensitivity of simulated climate to two atmospheric models: interpretation of differences between dry models and moist models. Monthly Weather Rev. 141 (5), 1558–1576. doi:10.1175/MWR-D-11-00367.1.

Zhang, X.H., 1990. Dynamical framework of IAP nine-level atmospheric general circulation model. Adv. Atmos. Sci. 7 (1), 67–77. doi:10.1007/BF02919169.